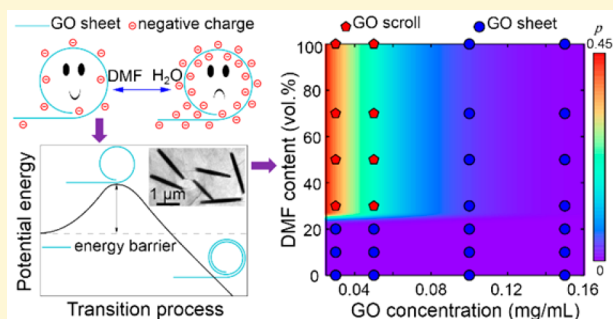


Transition of Graphene Oxide from Nanomembrane to Nanoscroll Mediated by Organic Solvent in Dispersion

Bo Tang,[†] Enlai Gao,^{‡,§,ID} Zhiyuan Xiong,[†] Bin Dang,[§] Zhiping Xu,^{*,‡,§,ID} and Xiaogong Wang^{*,†,ID}[†]Department of Chemical Engineering, Laboratory of Advanced Materials (MOE), Tsinghua University, Beijing 100084, P. R. China[‡]Applied Mechanics Laboratory, Department of Engineering Mechanics and Center for Nano and Micro Mechanics, Tsinghua University, Beijing 100084, P. R. China[§]State Key Laboratory of Power System, Department of Electrical Engineering, Tsinghua University, Beijing 100084, P. R. China

Supporting Information

ABSTRACT: Morphological transition of two-dimensional (2D) nanomembranes, where multiple factors such as thermal fluctuation, wrinkling, crumpling, and the intersheet adhesion play competitive roles, is a fascinating and intriguing problem with both fundamental and applied interests. In this work, we find that the morphological transition from graphene oxide (GO) nanomembranes to nanoscrolls can be mediated by *N,N*-dimethylformamide (DMF) in DMF-H₂O dispersions. As the DMF content is in the range from 30 vol % to 100 vol %, GO membranes are rolled up to form nanoscrolls in the low GO concentration regime (<0.05 mg/mL). The formed GO nanoscrolls show features of tight rolling-up with interlayer distance of 0.62 ± 0.04 nm and tubular structure with inner diameter of 5 nm. This morphological transition is proved to be controlled by the surface negative charges of the GO membranes in the dispersions. The electric double layer interaction, which hinders nanoscroll formation by introducing an electrostatic potential barrier in the scrolling nucleation and electrostatic repulsion between adjacent layers in the overlapping region during the rolling-up process, is significantly reduced by DMF. Theoretical analysis identifies the scrolling pathway through the energy barrier by considering the van der Waals interaction, electrostatic repulsion, elastic resistance of the membranes, and steric exclusion. A theoretical model that can predict the morphological phase diagram of GO in the space of the DMF content and GO concentration is established, which is essential to further explore the GO scroll formation in the dispersions for fundamental and applied researches.



INTRODUCTION

The morphological transition of two-dimensional (2D) nanomembranes has raised tremendous research interest in recent years because of their intriguing nature and great potential for real applications.^{1–6} As a unique type of the 2D nanomembranes, graphene oxide (GO) is featured by its pristine one-atom-thick aromatic lattice and oxidized domains with structural defects/vacancies, which include aliphatic six-membered rings, hydroxyl, epoxy, and carboxyl groups.^{7–10} Reduced graphene oxide (RGO), an analogue of graphene, can be fabricated from GO in large scale by chemical reduction for various applications.^{7,11} Meanwhile, GO with functional groups at graphene basal plane and edges with varied oxidation degrees is an ideal model material to explore the morphological transition of 2D membranes in dispersions.^{6,12} Typically, GO nanomembranes with finite in-plane elasticity and bending resistance display a nearly planar morphology, while thermal fluctuation or the presence of intrinsic defects can lead to the morphological phase transition.^{6,10,12} For GO nanomembranes suspended in dispersion media, their open edges are free and allowed for different bending modes with large magnitude, which could dominate their thermal fluctuation pattern under

proper conditions.⁶ The existence of the functional groups and defects/vacancies in the 2D crystal lattice will tune the interaction of GO membranes with the dispersion media, which can promote or inhibit the bending modes. Understanding of the morphological transition and phase diagram of GO in dispersions is critically important to further explore the chemical/physical behavior of GO and guide fundamental and applied researches.

The planar GO membranes and tubular nanoscrolls are two typical morphologies that can exist in dispersions.^{8,10,13} In the past decade, dispersion of GO in solvents has attracted much attention for modifying GO with functional groups,^{14–19} and mass fabrication of reduced graphene oxide (RGO) via chemical, thermally mediated or electrochemical reduction.^{11,16,17,20} Water is a solvent with the unique advantages such as cheap and environment-friendly for large-scale processing.^{7,10} GO membranes can be stably dispersed in water to possess a nearly planar morphology due to the

Received: May 16, 2018

Revised: August 13, 2018

Published: August 13, 2018

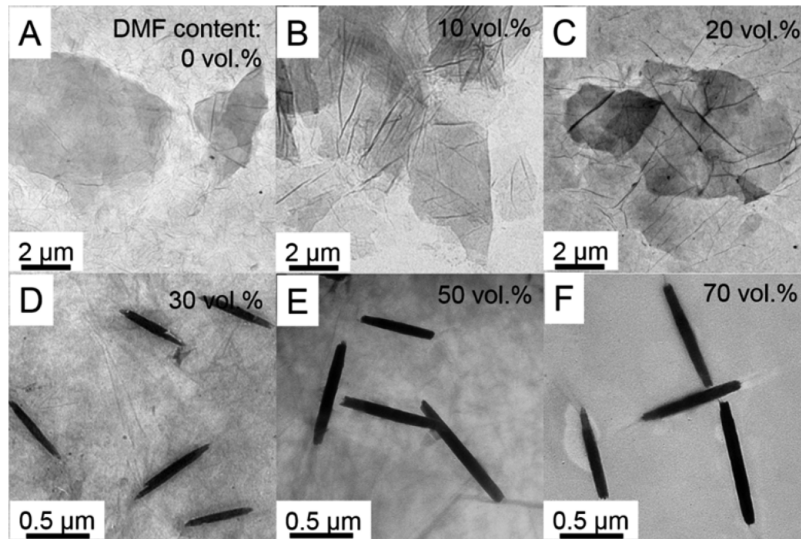


Figure 1. TEM images of the GO morphologies existing in the dispersions with the different DMF contents, from (A) to (F) $\psi = 0, 10, 20, 30, 50$, and 70 vol %.^{8,21,24–26}

presence of surface negative charges from carboxyl and hydroxyl groups.^{21,22} Planar GO membranes have also been observed to form the isotropic, liquid-crystal, and gel phases at different concentrations,^{23,24} which can be further processed into monolayers, fibers, films, and other forms.^{8,21,24–26} In the processes, the density of functional groups on individual platelets, the water content and drying condition can play important roles to affect the structure and properties of the final GO materials.^{27–29} On the other hand, under proper conditions, GO membranes can transform from a planar morphology to nanoscrolls through different approaches.^{30–36} Compared to the extremely flexible 2D membrane, the nanoscroll is known as the one-dimensional (1D) nanostructure. Carbon nanoscrolls have exhibited excellent performances in a wide spectrum of applications such as lubrication,³⁷ hydrogen storage,³⁸ and gas sensing.³⁹ The tight-rolled nanoscrolls with a tubular structure and ordered interlayer gallery can be expected for applications in filtration and separation processes by selective mass transport.^{40–42} Previous studies have shown that carbon nanoscroll formation from graphene is controlled by two opposite energetic contributions, where bending the graphene sheet causes the elastic energy increase and the van der Waals interaction in overlapping regions of the graphene sheets reduces the free energy.^{43,44} However, due to the existence of the oxidized domains with structural defects/vacancies and various functional groups, the scrolling process of the GO membranes in dispersion media is much more complicated and less understood. To our knowledge, despite the widely spreading interests and few preliminary results, the understanding of the morphological transition behavior of GO in dispersions and its phase diagram have not yet been reported in the literature.

In this work, we report the morphological transition of GO from nanomembranes to nanoscrolls mediated by *N,N*-dimethylformamide (DMF) in DMF-H₂O dispersions. The phase behavior of GO is controlled by GO concentration, energy barrier in the nanoscroll nucleation, and competition of the elastic resistance of the GO sheets, electrostatic and van der Waals interactions in the overlapping regions. The energy barrier in the nanoscroll nucleation and electrostatic interaction in the overlapping regions are found to be

significantly modified by DMF. Aligning with our experimental findings, a theoretical model is established to predict morphology phase diagram of GO in the space of the DMF content and GO concentration in the dispersions.

■ RESULTS AND DISCUSSION

We first experimentally explored the morphological transition of GO from nearly flat nanomembranes to nanoscrolls. Monolayer GO sheets were fabricated via the modified Hummers' method and characterization results of the GO samples are given in Figure S1 (Supporting Information, SI). The freeze-dried GO sample possessed the porous and loosely stacking structure (Figure S2), which could be easily exfoliated and dispersed in water after sonication. Although no 1D nanostructures were perceived in the freeze-dried GO sample, the formation of nanoscrolls was readily observed by dispersing the freeze-dried GO sample in H₂O-DMF media with a relatively high DMF content. Figure 1 shows the typical case of the morphological transition induced by DMF with the different contents (ψ) at the GO concentration (c) of 0.03 mg/mL. The membrane to scroll transition occurs with the relatively high DMF contents for the GO samples after being sonicated (40 kHz, 200 W) for 2 h. GO membranes keep their nearly planar morphology in water (Figure 1A), which is consistent with the previous reports.^{7,10,15} The membrane morphology is also observed for GO existing in the dispersions with $\psi = 10$ and 20 vol % (Figure 1B, C). However, as ψ increases to 30, 50, and 70 vol %, the morphological transition of GO from membranes to 1D nanostructures is clearly demonstrated (Figures 1D–F and S3A). The transition from nanomembranes to 1D nanostructures is reversible for those scrolls formed in the DMF-H₂O dispersion. As shown in Figure S3B, the scrolls formed in the dispersion with ψ of 30 vol % revert to the original membrane state when ψ is reduced to 5 vol %.

To confirm that DMF has the effect to induce the scroll formation, the freeze-dried GO sample was dispersed in DMF (0.03 mg/mL) via sonication under the same condition. GO membranes were also observed to form scrolls in the DMF dispersion (Figures 2A, B) with the average length of ~2070 nm (Figure S4). But, it should be noted that there are some

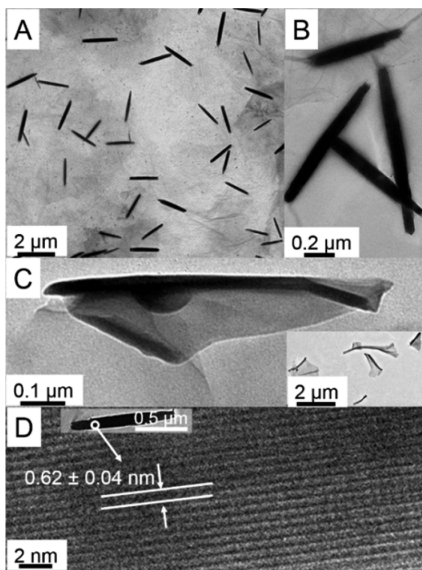


Figure 2. (A, B) The TEM images of the GO nanoscrolls formed by dispersing the freeze-dried GO sample in DMF, (C) the intermediate state of the scroll formation, and (D) the high-resolution TEM image of a typical nanoscroll.

GO membranes with relatively large size that cannot be rolled up in the process as shown in Figure 2A. Because the initial bending energy barrier is closely related to the rolling width, DMF can only induce the GO membranes with relatively small sizes to curl up to form nanoscrolls.¹³ Therefore, the average length of the formed nanoscrolls is smaller than the average lateral size of the GO nanomembrane (Figure S4). Figure 2C shows a TEM image of the intermediate state of 1D nanoscroll formation in DMF dispersion, where roll-up from the edge can clearly be seen. The high-resolution TEM result of a typical GO nanoscroll suggests that it has the ordered interlayer gallery (Figure 2D), which differs to lose-packed nanoscrolls.^{30–35} The interlayer distance of 0.62 ± 0.04 nm is larger than those of MWCNT and graphene nanoscrolls (0.34 nm),^{45,46} owing to the existence of functional groups on the GO sheets. As the sizes of the scrolls are relatively large, which can be observed with an optical microscope (OM). Figure S5 shows the OM images of the GO nanoscrolls formed in the DMF dispersion. It confirms that nanoscrolls are formed in the dispersion, not from the drying process for the TEM observation. The inner structure was observed with the high-resolution TEM on a relatively small GO nanoscroll with the diameter about 30 nm for electron beam penetration (Figure S6A). The hollow structure with an inner diameter of about 5 nm can be clearly seen for the scroll formed through the rolling up. Figure S6B provides the Raman spectra of the GO nanoscrolls and GO sheets. The intensity ratio between the D band and G band of the GO nanoscrolls is 1.12, which is slightly larger compared to that of GO sheets (1.10). The G band of GO nanoscrolls is red-shifted from 1595 cm^{-1} (GO sheets) to 1589 cm^{-1} , which is consistent with the previous observation on GO nanoscrolls.³³ The above results all confirm that GO membranes are tightly rolled up to form GO nanoscrolls with ordered interlayer packing and a hollow core.

Figure 3A illustrates the scrolling process of the GO membrane, which is controlled by the competition between the bending resistance and face-to-face van der Waals interaction in the overlapping regions. The van der Waals

interaction between sheets can overcome the bending resistance, stabilize the newly formed nanoscroll nucleated by thermal fluctuation, and drive the following rolling-up process.^{43,44} For GO with oxygen-rich surface functional groups and basal-plane defects, the presence of defects facilitates the transition from flat sheets to nanoscrolls.^{6,12} As presented below in detail, our results show that the repulsive electric double-layer interaction of GO sheets in the dispersions is a critically important factor to control the morphology, which is determined by the DMF content in the dispersions (Figure 3B). The DMF content has effects on both the nucleation of a nanoscroll with the signature of the first cylinder and the continuous rolling-up process toward the final stable 1D nanoscrolls.

The surface negative charge density of the GO sheets, which is from the ionization of carboxylic groups and other negative charges on the surfaces, is determined from the zeta potential of GO membrane based on the Gouy–Chapman equation:²²

$$\sigma = \frac{2\epsilon_m \epsilon_0 k k_B T}{ze} \sinh(ze\xi/2k_B T) \quad (1)$$

where σ is the surface charge density, ϵ_m is the relative dielectric constant of the H_2O –DMF mixture, ϵ_0 is the permittivity of vacuum, k is the reciprocal of Debye screening length (m^{-1}), z is the valence of the counterions, e is the unit charge ($1.6 \times 10^{-19}\text{ C}$), and ξ is the average zeta potential of GO sheets. Here, ϵ_m is calculated as $\epsilon_m = x_{\text{water}}\epsilon_{\text{water}} + (1 - x_{\text{water}})\epsilon_{\text{DMF}}$, where x_{water} is the volume fraction for water, ϵ_{water} and ϵ_{DMF} are the relative dielectric constants of water and DMF ($\epsilon_{\text{water}}, 80.1$; $\epsilon_{\text{DMF}}, 36.7$).^{47,48} As shown in Figure 3C, the absolute value of ξ is 50.3 ± 6.4 mV for GO in water ($\text{pH} = 7$, $c = 0.03\text{ mg/mL}$), which declines rapidly from 50.3 ± 6.4 to 18.2 ± 4.3 mV with ψ increasing from 0 to 30 vol %, then slowly decreases to 12.6 ± 3.9 , 9.1 ± 2.1 , and 7.3 ± 2.1 mV as ψ further increases to 50, 70, and 100 vol %. According to the reported σ of 0.625 e/nm^2 (100 mC/m^2) for ξ of GO in water (-50 mV),²² the value of κ can be obtained from eq 1, which is used to calculate other σ values. As shown in Figure 3D, the normalized σ (NCD) of the GO membranes is reduced with the increase of ψ . The electrostatic potential barrier in the nucleation and the electrostatic repulsion in the overlapping regions will hinder the morphological transition from planar GO membranes to scrolls. DMF as an organic solvent is unfavorable for the ionization of carboxylic groups and also prevents the association of water molecules on the GO surface to form the “iceberg” structure. As the negative charge density of GO is reduced by DMF, GO sheets can overcome the energy barrier in the nanoscroll nucleation. Meanwhile, the electrostatic repulsion in the overlapping regions is also reduced in the following rolling-up process, which can be overcome by the van der Waals interaction in the overlapping regions of GO membranes. The statements are quantitatively verified by the results from calculations and experiments as discussed below.

The electrostatic potentials (EP) are calculated by using COMSOL Multiphysics software for the nucleation of planar membrane to form the first roll of the scroll. Figure 3E shows the result for the nanoscroll nucleation of a typical GO membrane with the size of $2070 \times 2070\text{ nm}^2$, which is based on the average length of GO nanoscrolls (Figure S4). The effect of initial radius (r_0) on the electrostatic potential barrier (EPB) of nanoscroll nucleation is explored as shown in Figure 3F, when ψ is 100 vol %. It indicates that EPB has the positive

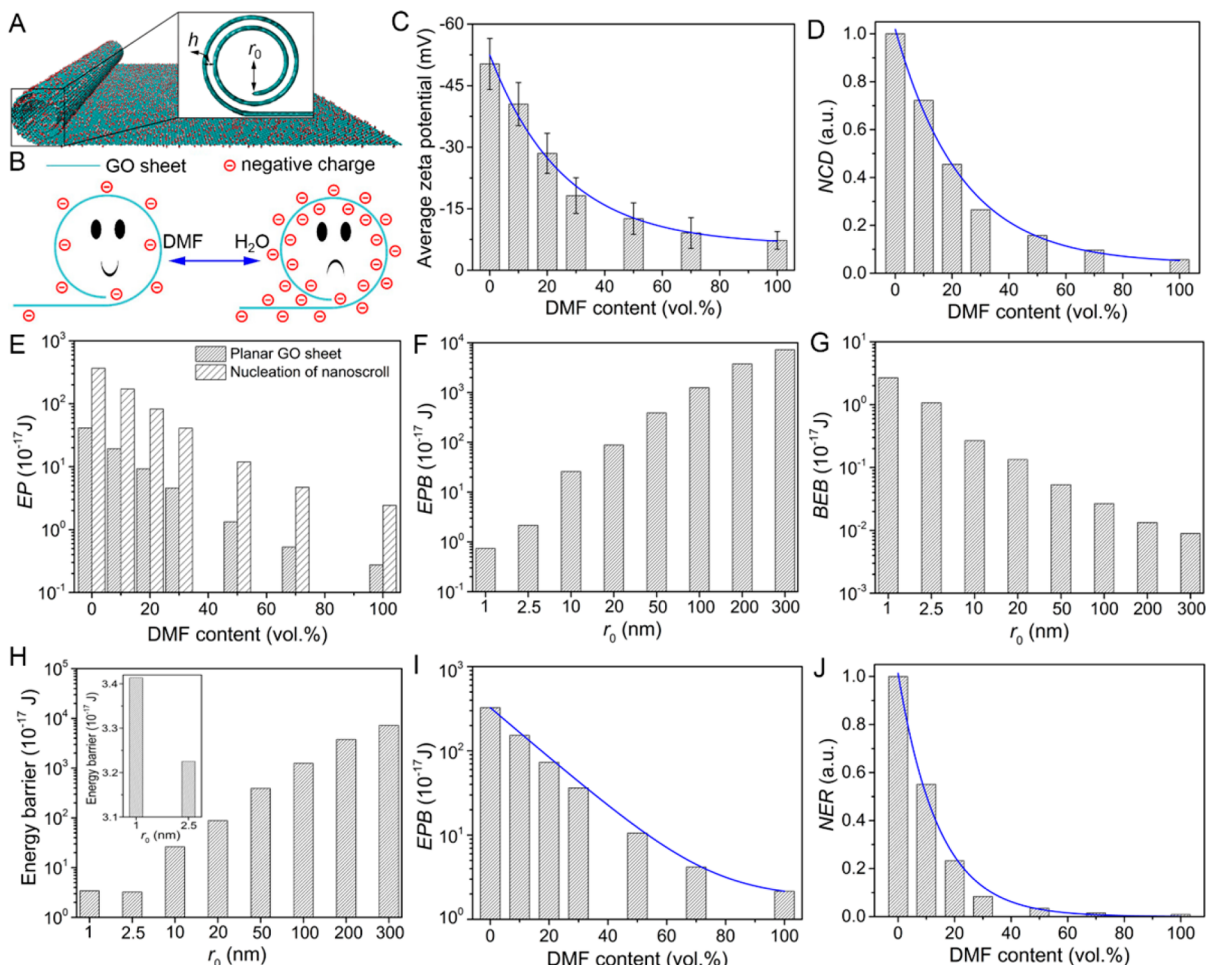


Figure 3. (A) The schematic illustration of nanoscroll formation from GO membrane, (B) the cartoon of nanoscroll nucleation from an isolated GO sheet with low (left) and high (right) surface charge densities, (C) the average zeta potential of GO membranes measured at varying DMF contents, (D) the relation between normalized charge density (NCD) of GO sheets and DMF content, (E) the electrostatic potential (EP) of planar GO membrane and scroll nucleation obtained by COMSOL Multiphysics calculation, (F) the electrostatic potential barrier (EPB) in the nucleation of nanoscrolls with different initial radius (r_0), (G) the bending energy barrier (BEB) in the nucleation of nanoscrolls with different r_0 , (H) the total energy barrier of electrostatic potential and bending energy in the nucleation of nanoscrolls with different r_0 , (I) EPB for the nucleation of nanoscrolls at various DMF contents, and (J) the relation between the normalized electrostatic repulsion (NER) in the overlapping regions of GO membranes and DMF content.

Table 1. Electrostatic Repulsion and van der Waals Interaction Energy in the Overlapping Regions of GO Sheets during the Nanoscroll Formation

DMF content (vol.%)	0	10	20	30	50	70	100
ΔW	>0	>0	>0	<0	<0	<0	<0
electrostatic repulsion ^a	2.60	1.43	0.60	0.22	0.09	0.03	0.02
bending energy ^a	0.78	0.78	0.78	0.78	0.78	0.78	0.78
van der Waals ^a	1.33	1.28	1.23	1.18	1.09	1.00	0.86

^aThe energy unit is 10^{-3} J/m².

correlation with r_0 . Figure 3G exhibits that the bending energy barrier (BEB) decreases with r_0 when ψ is 100 vol % (see the SI for more details). As shown in Figure 3H, the total energy barrier including EPB and BEB is the lowest as r_0 is about 2.5 nm, which is also consistent with the experimental result (Figure S6A). Hence, r_0 is taken as 2.5 nm to calculate EPB for different ψ . Figure 3I shows that EPB decreases with the ψ increase from 0 to 100 vol %, when the bending energy is the constant value as r_0 is fixed as 2.5 nm. It suggests that the nucleation of nanoscrolls is easier with the increase of ψ for the lower total energy barriers.

After the nucleation of the nanoscrolls, the morphological transition of GO from flat membranes to the final nanoscrolls can be characterized by the following:

$$\Delta W = W_e + W_b - W_{vdW} \quad (2)$$

where W_e and W_{vdW} are the electrostatic repulsion energy and van der Waals interaction between GO sheets in the overlapping regions, and W_b is the bending energy of GO sheets. W_e can be obtained via the following:¹⁹

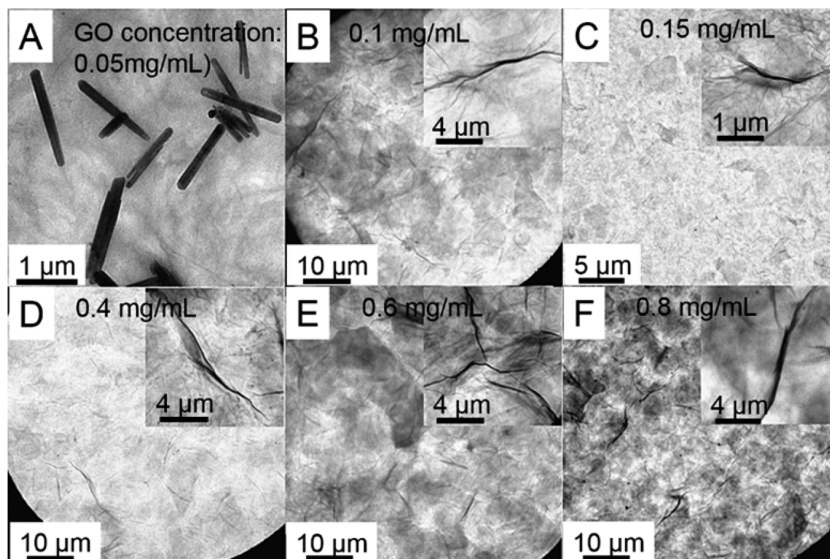


Figure 4. TEM images of the nanoscrolls and GO membranes separated from the DMF dispersions with the different GO concentrations indicated.

$$W_e = \frac{2\sigma^2}{\kappa\epsilon_m\epsilon_0} \exp(-\kappa h) \quad (3)$$

where h is the spacing distance between GO sheets. Figure 3J shows that the normalized W_e declines rapidly with ψ . The value of W_e here is calculated to be 2.60×10^{-3} J/m² for $h = 0.62$ nm as ψ is 0 vol %, W_{vdw} is calculated to be 1.33×10^{-3} J/m² for $h = 0.62$ nm (see the SI for more details), and the maximal value of $W_b = D/2r_0^2$ is 7.81×10^{-4} J/m² by considering the fact that $r_0 = \sim 2.5$ nm (Figure S6A), where D is the bending stiffness of GO sheets ($1k_B T$).⁴⁹ From the date listed in Table 1, we conclude that the nanoscrolls cannot form in water as W_{vdw} is not big enough to overcome the energy barriers resulting from W_b and W_e ($\Delta W > 0$). In other words, the high σ introduces a significant energy barrier for the formation of nanoscrolls. The morphological transition of GO is absent for ψ of 10 and 20 vol % as $\Delta W > 0$. However, as ψ increases to 30, 50, 70, and 100 vol %, the formation of nanoscrolls is favored in energy as σ and W_e are significantly reduced, signaled by $\Delta W < 0$. Moreover, the radius of curvature of nanoscrolls increases as scrolling proceeds, and W_b will become smaller and the potential energy becomes even lower for $\Delta W < 0$, which indicates that the final state of the nanoscrolls has the lower energy compared to that of planar membranes as shown in Figure S7.

As indicated by previous theoretical studies without considering the solvent effect, a stable equilibrium core size of CNS should depend on the basal graphene length, the interlayer spacing, the interaction energy between layers of CNS and the bending stiffness of graphene.^{50–52} It has also been reported that the stacking manner of GO sheets is closely related to the water content and drying condition.^{27,28} These factors could similarly affect the core size. Our above calculation shows that after the nanoscroll nucleation, the scroll formation is the downhill process, where the potential energy decreases with the rolling length (Figure S7, see the SI for details). Therefore, the core size should mainly be determined by the initial value (r_0). As shown in Figure 3H, the total potential energy for the nucleation shows a shallow minimum around 2.5 nm, and the core size could be varied in a range around this value under different conditions. As the

possible variation of the core size is relatively small (few nanometers), which is also consistent with the previous studies,^{50,52} the value $r_0 = 2.5$ nm is adopted for the following discussion. This approximation is in the same accuracy order as the others used in this study.

To further verify the critically important role of the electrostatic potential barrier, the freeze-dried GO sample was also purposefully dispersed in an aqueous medium ($c = 0.03$ mg/mL) with pH = 2.2 by adding a suitable amount of HCl, the absolute value of ξ for the GO membranes is decreased from 50.3 ± 6.4 to 22.9 ± 2.7 mV and σ is reduced accordingly (Figure S8A). As predicted by the calculation, GO nanoscroll formation is observed in the dispersions (Figures S8B–E and S9). It confirms the key role of the repulsive double layer interaction in the morphological transition of GO, which can be adjusted by adding an organic solvent or inorganic acid.

Another remarkable observation of this study is that the membrane-to-scroll transition of GO is controlled by the GO concentration in the dispersion media (Figure 4). GO nanoscrolls can be ubiquitously observed in the DMF dispersions with $c = 0.03$ and 0.05 mg/mL (Figures 2 and 4A), but are absent for $c = 0.1, 0.15, 0.4, 0.6$, and 0.8 mg/mL. As shown in Figures 4B–F, GO membranes touch with each other and only crumples are observed instead of any signature of scrolling. To confirm this observation, we extended our investigation to various ψ , and find that as ψ arrives at 30, 50, and 70 vol %, the transition into nanoscrolls can only be observed at $c = 0.05$ mg/mL, but not for the dispersion with the higher concentration such as $c = 0.1$ and 0.15 mg/mL (Figures S10–S12). This value below $c = 0.1$ mg/mL for the formation of nanoscrolls is consistent with the result that the nanoscroll formation from reduced graphene oxide (RGO) occurs only in the low concentration region.⁵³ The effect of GO concentration on the scroll formation is also observed for other organic solvents, such as pyridine, methanol, isopropyl alcohol, ethanol, isobutyric acid, and acetic acid.¹³

As discussed above, one of the key factors controlling the morphological transition of GO is electric double-layer interaction, which is quantified by ξ of GO membranes. Our measurements show that ξ is insensitive to c at the fixed ψ

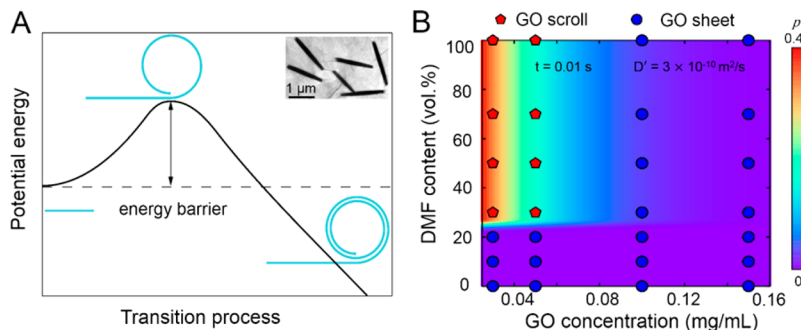


Figure 5. (A) The energy barrier for the scrolling of GO; (B) the morphological phase diagram of GO.

(Figure S13), which verifies that the c effect on the scroll formation is irrelevant with EPB in the scroll nucleation and W_e between layers in the overlapping regions. As reported in the literature, the GO dispersion demonstrates nematic and gel phases at $c > 0.05$ mg/mL, where no scroll formation can be observed.^{23–25} A vital difference between these phases and the diluted dispersion concerned in this study is the spatial distance between GO membranes. In a GO dispersion with relatively high concentration, the spatial distance is small and GO membranes strongly interact with each other to form sandwich-like structures of GO-water-GO as W_e is reduced, where the bending barrier cannot be overcome by W_{vdW} to cause scrolling.^{54,55} In the diluted dispersion, it is difficult for the GO membranes to aggregate and form the GO–water–GO structures via the face-to-face pattern, while rolling up to form nanoscrolls is more preferable with the reduced EPB, W_e and $\Delta W < 0$.

On the basis of the above understanding, a morphological phase diagram of GO in the space of GO concentration and DMF content is obtained through the following approach. As discussed above, the formation of GO nanoscrolls is energetically favorable and spontaneous after the scroll nucleation. While the nucleation of nanoscrolls from isolated GO membranes has to overcome the total energy barrier from the elastic bending and EPB (Figure 5A). To proceed to the formation of GO nanoscroll, two criteria have to be met: (1) isolation of individual GO membranes in the dispersion; (2) nanoscroll nucleation with a reasonably high probability through the dynamic process, which are presented below, respectively.

First, the isolation condition is determined from steric consideration, and the probability of isolated GO sheets (p_i) is identified as follows:

$$p_i = \left(1 - \frac{\alpha \Delta V}{V}\right)^N = \left[\left(1 - \frac{\alpha \Delta V}{V}\right)^{V/\alpha \Delta V}\right]^{\alpha \phi} \quad (4)$$

where ΔV is the average volume for a piece of GO sheet, V is the volume of GO dispersion, $\phi = N\Delta V/V$ is the volume fraction of GO sheets, N is number of GO sheets, and α is a dimensionless factor, defined as the ratio between the activated space of one GO sheet (V_a) and ΔV ($V_a = \alpha \Delta V$). Here V_a is related to the Brownian motion of GO sheets, which can be obtained from the following:

$$V_a(t) = \frac{4}{3}\pi(\sqrt{\langle r^2 \rangle})^3 = \frac{4}{3}\pi(\sqrt{6D't})^3 \quad (5)$$

where D' is the translational diffusion coefficient of a GO sheet, t is time, and r is the diffusion length that the center of

mass of GO sheets travels during t . Meanwhile, ΔV is about 4.4×10^{-21} m³ considering that the average area for one piece of GO sheet is ~ 8.6 μm² (Figure S4A). As $V_a \ll V$, so eq 4 can then be written as follows:

$$p_i = \left[1 - \alpha(t, D') \frac{\Delta V}{V}\right]^N = \exp[-\alpha(t, D')\phi] \quad (6)$$

By neglecting the density difference between DMF and water, ϕ can be linearly related to c for specific ψ (0.05 mg/mL vs 2.27×10^{-5}).²³ p_i can thus be expressed as $p_i(t, D', c)$.

Second, to obtain the condition for overcoming the energy barrier of the nucleation, we evaluate the probability of nanoscroll nucleation (p_n) from a reduced 2D model with a GO nanoribbon, the width of which is the lattice constant of graphene (0.24 nm), and the thermal fluctuation on the order of $k_B T$ is the driving force for the nanoscroll nucleation. The simplification into a 2D model is valid because once one bending mode of the nanoribbon is activated, displacive fluctuation in the perpendicular directions will be suppressed.⁶ On the basis of the First-Passage-Time (FPT) model, p_n from 2D GO nanoribbons can be expressed as follows:

$$p_n = 1 - \left[1 - \exp\left(-\frac{E_e + E_b}{k_B T}\right)\right]^{ft} \quad (7)$$

where E_e and $E_b = \sim 0.3 k_B T$ are the electrostatic potential barrier and the bending energy barrier in the nanoscroll nucleation from the GO nanoribbon, $f = 1.49 \times 10^8$ s⁻¹ is its natural flexural frequency in the bending mode of GO nanoribbon (see SI for details), which is the number of attempts to nucleate a nanoscroll per second. The results show that E_e depends on ψ (Figures 3J and S14), and p_n can then be expressed as follows:

$$p_n(t, \psi) = 1 - \left[1 - \exp\left(-\frac{E_b + E_e(\psi)}{k_B T}\right)\right]^{ft} \quad (8)$$

Hence, the probability of nanoscroll nucleation from isolated GO sheets (p) is expressed as follows:

$$p = p_i(t, D', c) \times p_n(t, \psi) \quad (9)$$

and the morphological phase diagram of GO is then constructed by using eq 9. The theoretical prediction based on the criterion of the nanoscroll nucleation can be directly compared to the experimentally identified phase diagram. As shown in Figure 5B, the theoretical results suggest that p is relatively high in the top-left region of the diagram with relatively high ψ and low c , where the experimental observation

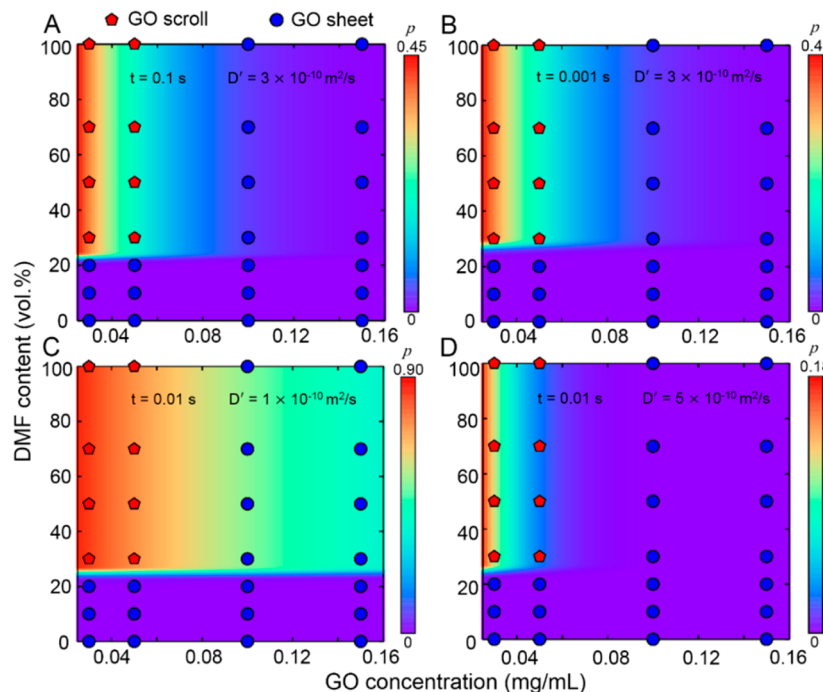


Figure 6. Morphological phase diagram of GO nanoscrolls for the different time lapse and translational diffusion coefficients of the GO sheets.

on GO nanoscrolls is well identified. This set of parameters $t = 0.01$ s and $D' = 3 \times 10^{-10}$ m²/s is chosen to match experimental observations on the scroll formation at $c = 0.03$ and 0.05 mg/mL, where the condition of $\Delta W < 0$ is fulfilled for $\psi > 20$ vol.%. In contrast, p is extremely low, approaching zero, at $c = 0.1$ and 0.15 mg/mL, and the scroll formation is absent.

We also explore the morphological phase diagram of GO over different t and D' , and the results are summarized in Figures 6 and S15. The morphological phase diagram can be distinctly modified by changing these two parameters. As t increases to 0.1 s while D' is fixed at 3×10^{-10} m²/s, the critical ψ for morphological phase transition reduced to ~ 20 vol.% (Figure 6A), which can be explained by the fact that p_n increases with time at the same ψ , as predicted by eq 8, while the critical ψ for morphological phase transition increases to ~ 30 vol.% as t decreases to 0.001 s (Figure 6B). Although the formation of nanoscrolls could be a reversible process, the decrease of the potential energy in the scrolling process is much larger in magnitude than the total energy barrier in the nanoscroll nucleation and then GO nanoscrolls tend to form at the long time limit. However, Figure 6C, D present the morphological phase diagrams of GO nanoscroll for different D' at the fixed value of $t = 0.01$ s, which is reasonable as discussed above. When D' decreases to 1×10^{-10} m²/s, the critical c for morphological phase transition becomes higher than 0.15 mg/mL, which is not consistent with the experimental results. It can be explained by the fact that p_i increases as D' is reduced at the fixed c (eqs 4, 5, and 6). Meanwhile, the critical c for morphological phase transition becomes lower than 0.05 mg/mL as D' increases to 5×10^{-10} m²/s, which is also against the experimental results. Therefore, D' can be reasonably adopted the value of 3×10^{-10} m²/s to match the morphological phase diagram of GO. The calculations prove that the set of parameters $t = 0.01$ s and $D' = 3 \times 10^{-10}$ m²/s can best fit our experimental results and be used for further investigations.

CONCLUSIONS

In this work, the morphological transition of GO from planar membranes to nanoscrolls in DMF-H₂O dispersions is elucidated by considering the effects of DMF and GO concentration. The surface charge density of GO membranes decreases as the DMF content increases from 0 to 100 vol.%, which reduces both the electrostatic potential barrier in the nucleation of nanoscrolls and the electrostatic repulsion in the overlapping regions in the nanoscroll formation. GO remains the planar morphology at the low DMF content (0, 10, and 20 vol.%), but transition into nanoscrolls is activated at the DMF content higher than 20 vol.%. In addition, the nanoscroll formation depends on the GO concentration that defines the isolation condition of the dispersed GO membranes. Nanoscrolls are barely observed when the GO concentration is higher than 0.1 mg/mL. Finally, the morphological phase diagram of GO in the space of the DMF content and GO concentration is obtained by the theoretical analysis and calculation, which can be employed to explore the phase behavior of GO in dispersions and guide the fabrication of GO nanoscrolls in large scale.

EXPERIMENTAL SECTION

Preparation of GO. The modified Hummers' method was employed to fabricate GO sample.^{14,56–58} Under the condition of ice-bath cooling, 300 mesh graphite power (3.0 g) and potassium nitrate (3.6 g) were added into the concentrated sulfuric acid (138 mL). After the mixture was stirred for 30 min, potassium permanganate (18 g) was slowly added. Then the mixture was placed in an oil-bath (35 °C) for 48 h. Then, excess water (300 and 1500 mL in two batches) was slowly added with ice-bath cooling, and 18 mL H₂O₂ (30%) was dropwise added with the color change from brown to yellow. The GO dispersion was repeatedly washed with abundant water and concentrated by the centrifuge with the speed of 18 000 rpm for 30 min until pH reached about 7. The concentrated GO was obtained by the centrifuge at the speed of 6000–12 000 rpm for 30 min. Finally, GO sample was obtained from the concentrated GO via freeze-drying for 24 h.

Morphology Transition Study. DMF with spectral purity and HCl (36.5% water solution) were purchased from Sigma-Aldrich. A Milli-Q water purification system was employed to prepare the deionized water (resistivity >18 MΩ·cm). The morphological transition was studied by dispersing the freeze-dried GO in DMF-H₂O media with different DMF contents via sonication (40 kHz, 200 W, 2 h). For comparison, the freeze-dried GO was also dispersed in water with pH of 2.2 via adding HCl. The dispersions without further treatment were dropped onto the copper TEM grids. Before TEM observation, the samples were exposed to the air under ambient condition to evaporate the dispersion media for 24 h and dried under vacuum for 12 h at room temperature.

Characterization. Atomic force microscopy (AFM), X-ray diffraction (XRD), X-ray photoelectron spectroscopy (XPS), and Raman spectroscopy were employed to investigate GO. The single-layer GO sheets were confirmed by an AFM apparatus from Bruker Corporation (Dimension ICON-PI). The used probe had a tip radius of 6~8 nm, and the tapping mode was adopted in the experiment with an amplitude set-point about 340 mV. XRD curves were obtained from a Bruker D8 Advance X-ray diffractometer with Cu K α radiation (1.5406 Å). The binding energy of the elements was observed by an X-ray photoelectron spectrometer (ESCALAB250Xi) using a monochromatized Al K α X-ray source of 1486.6 eV under normal incidence. A Renishaw 1000 microspectrometer with an excitation wavelength of 633 nm was used to obtain Raman spectra. The zeta potentials of GO membranes in the dispersions were measured by Malvern Zetasizer Nano. A field-emission scanning electron microscope (SEM: Zeiss Merlin, 5.0 kV) was employed to investigate the freeze-dried GO and nanoscrolls. The TEM observations of GO membranes and GO nanoscrolls were realized via Hitachi H-7650B with the electron beam of 80 kV. The high-resolution TEM images of nanoscrolls were obtained by JEM2010 (03006800) with the electron beam of 120 kV. Optical microscopic images were captured by a Nikon LV 100 POL microscope equipped with Nikon DS-Fi2 CCD camera.

■ ASSOCIATED CONTENT

S Supporting Information

The Supporting Information is available free of charge on the ACS Publications website at DOI: [10.1021/acs.chemmater.8b02083](https://doi.org/10.1021/acs.chemmater.8b02083).

AFM, XRD, XPS, and Raman investigations of GO sheets; SEM images of the freeze-dried GO sample; TEM images of GO nanoscrolls and GO membranes; size distribution of GO sheets and length distribution of GO nanoscrolls; optical microscopic images; high-resolution TEM and Raman spectra of GO nanoscrolls; the potential energy of scrolling GO membranes; relationship between surface charge density and zeta potential of GO membranes; GO nanoscrolls formed in aqueous dispersion with the pH of 2.2; morphological transition from GO membranes to nanoscrolls (0.05 mg/mL); TEM images of GO membranes ($c = 0.1$ and 0.15 mg/mL); zeta potentials of GO sheets for different GO concentrations at various DMF contents; the electrostatic potential barrier for the nucleation of nanoscrolls for GO nanoribbon; morphological phase diagram of GO; the calculations of energy barrier for nanoscroll nucleation; van der Waals interaction between adjacent sheets in the overlapping regions; potential energy of scrolling GO sheets and natural flexural frequency of GO sheets ([PDF](#))

■ AUTHOR INFORMATION

Corresponding Authors

*Tel: +86 10 62796171. E-mail: wxg-dce@mail.tsinghua.edu.cn (X.W.).

*Tel: +86 10 62798274. E-mail: xuzp@tsinghua.edu.cn (Z.X.).

ORCID

Enlai Gao: [0000-0003-1960-0260](http://orcid.org/0000-0003-1960-0260)

Zhiping Xu: [0000-0002-2833-1966](http://orcid.org/0000-0002-2833-1966)

Xiaogong Wang: [0000-0002-8721-6976](http://orcid.org/0000-0002-8721-6976)

Author Contributions

B.T and E.G. contributed equally to this work. B.T. accomplished the experiments of fabrications and observations on GO nanoscrolls, analyzed the data, and wrote the paper. E.G. employed the analysis and modeled the mechanism of GO nanoscroll formation, and wrote a part of the paper. Z.X. provided help to analyze the data. B.D. helped to calculate electrostatic potential barrier for scroll nucleation. X.W. and Z.X. supervised the project, and revised the paper. All authors discussed the results and made comments on the manuscript.

Notes

The authors declare no competing financial interest.

■ ACKNOWLEDGMENTS

This work was supported by NSFC under Projects 51773108 and 11472150.

■ REFERENCES

- (1) Geim, A. K.; Novoselov, K. S. The Rise of Graphene. *Nat. Mater.* **2007**, *6*, 183–191.
- (2) Lagally, M. G. Silicon Nanomembranes. *MRS Bull.* **2007**, *32*, 57–63.
- (3) Mei, Y. F.; Huang, G. S.; Solovev, A. A.; Ureña, E. B.; Mónch, I.; Ding, F.; Reindl, T.; Fu, R. K. Y.; Chu, P. K.; Schmidt, O. G. Versatile Approach for Integrative and Functionalized Tubes by Strain Engineering of Nanomembranes on Polymers. *Adv. Mater.* **2008**, *20*, 4085–4090.
- (4) Mei, Y. F.; Thurmer, D. J.; Deneke, C.; Kiravittaya, S.; Chen, Y. F.; Dadgar, A.; Bertram, F.; Bastek, B.; Krost, A.; Christen, J.; Reindl, T.; Stoffel, M.; Coric, E.; Schmidt, O. G. Fabrication, Self-Assembly, and Properties of Ultrathin AlN/GaN Porous Crystalline Nanomembranes: Tubes, Spirals, and Curved Sheets. *ACS Nano* **2009**, *3*, 1663–1668.
- (5) Cendula, P.; Kiravittaya, S.; Mónch, I.; Schumann, J.; Schmidt, O. G. Directional Roll-up of Nanomembranes Mediated by Wrinkling. *Nano Lett.* **2011**, *11*, 236–240.
- (6) Xu, Z. P.; Buehler, M. J. Geometry Controls Conformation of Graphene Sheets: Membranes, Ribbons and Scrolls. *ACS Nano* **2010**, *4*, 3869–3876.
- (7) Dreyer, D. R.; Park, S. J.; Bielawski, C. W.; Ruoff, R. S. The Chemistry of Graphene Oxide. *Chem. Soc. Rev.* **2010**, *39*, 228–240.
- (8) Stankovich, S.; Dikin, D. A.; Dommett, G. H. B.; Kohlhaas, K. M.; Zimney, E. J.; Stach, E. A.; Piner, R. D.; Nguyen, S. T.; Ruoff, R. S. Graphene-Based Composite Materials. *Nature* **2006**, *442*, 282–286.
- (9) Loh, K. P.; Bao, Q. L.; Eda, G.; Chhowalla, M. Graphene Oxide as A Chemically Tunable Platform for Optical Applications. *Nat. Chem.* **2010**, *2*, 1015–1024.
- (10) Cheng, C.; Li, D. Solvated Graphenes: An Emerging Class of Functional Soft Materials. *Adv. Mater.* **2013**, *25*, 13–30.
- (11) Park, S.; Ruoff, R. S. Chemical Methods for the Production of Graphenes. *Nat. Nanotechnol.* **2009**, *4*, 217–224.
- (12) Wallace, J.; Shao, L. Defect-Induced Carbon Nanoscroll Formation. *Carbon* **2015**, *91*, 96–102.
- (13) Tang, B.; Yun, X. W.; Xiong, Z. Y.; Wang, X. G. Formation of Graphene Oxide Nanoscrolls in Organic Solvents: Toward Scalable Device Fabrication. *ACS Appl. Nano Mater.* **2018**, *1*, 686–697.

- (14) Hummers, W. S.; Offeman, R. E. Preparation of Graphitic Oxide. *J. Am. Chem. Soc.* **1958**, *80*, 1339–1339.
- (15) Paredes, J. I.; Villar-Rodil, R. S.; Martinez-Alonso, A. A.; Tascon, J. M. D. Graphene Oxide Dispersions in Organic Solvents. *Langmuir* **2008**, *24*, 10560–10564.
- (16) Stankovich, S.; Piner, R. D.; Nguyen, S. T.; Ruoff, R. S. Synthesis and Exfoliation of Isocyanate-Treated Graphene Oxide Nanoplatelets. *Carbon* **2006**, *44*, 3342–3347.
- (17) Park, S.; An, J.; Jung, I.; Piner, R. D.; An, S. J.; Li, X.; Velamakanni, A.; Ruoff, R. S. Colloidal Suspensions of Highly Reduced Graphene Oxide in A Wide Variety of Organic Solvents. *Nano Lett.* **2009**, *9*, 1593–1597.
- (18) Konios, D.; Stylianakis, M. M.; Stratakis, E.; Kymakis, E. Dispersion Behavior of Graphene Oxide and Reduced Graphene Oxide. *J. Colloid Interface Sci.* **2014**, *430*, 108–112.
- (19) Gudarzi, M. M. Colloidal Stability of Graphene Oxide: Aggregation in Two Dimensions. *Langmuir* **2016**, *32*, 5058–5068.
- (20) Eda, G.; Chhowalla, M. Chemically Derived Graphene Oxide: Towards Large-Area Thin-Film Electronics and Optoelectronics. *Adv. Mater.* **2010**, *22*, 2392–2415.
- (21) Li, D.; Müller, M. B.; Gilje, S.; Kaner, R. B.; Wallace, G. G. Processable Aqueous Dispersions of Graphene Nanosheets. *Nat. Nanotechnol.* **2008**, *3*, 101–105.
- (22) Konkena, B.; Vasudevan, S. Understanding Aqueous Dispersion of Graphene Oxide and Reduced Graphene Oxide through pH Measurements. *J. Phys. Chem. Lett.* **2012**, *3*, 867–872.
- (23) Naficy, S.; Jalili, R.; Aboutalebi, S. H.; Gorkin III, R. A.; Konstantinov, K.; Innis, P. C.; Spinks, G. M.; Poulin, P.; Wallace, G. G. Graphene Oxide Dispersions: Tuning Rheology to Enable Fabrication. *Mater. Horiz.* **2014**, *1*, 326–331.
- (24) Xu, Z.; Gao, C. Graphene Chiral Liquid Crystals and Macroscopic Assembled Fibres. *Nat. Commun.* **2011**, *2*, 571.
- (25) Xiao, Y. H.; Xu, Z.; Liu, Y. J.; Peng, L.; Xi, J. B.; Fang, B.; Guo, F.; Li, P.; Gao, C. Sheet Collapsing Approach for Rubber-like Graphene Papers. *ACS Nano* **2017**, *11*, 8092–8102.
- (26) Zhang, M.; Wang, Y. L.; Huang, L.; Xu, Z. P.; Li, C.; Shi, G. Q. Multifunctional Pristine Chemically Modified Graphene Films as Strong as Stainless Steel. *Adv. Mater.* **2015**, *27*, 6708–6713.
- (27) Medhekar, N. V.; Ramasubramaniam, A.; Ruoff, R. S.; Shenoy, V. B. Hydrogen Bond Networks in Graphene Oxide Composite Paper: Structure and Mechanical Properties. *ACS Nano* **2010**, *4*, 2300–2306.
- (28) Hong, S. H.; Shen, T. Z.; Song, J. K. Water Front Recession and the Formation of Various Types of Wrinkles in Dried Graphene Oxide Droplets. *Carbon* **2016**, *105*, 297–304.
- (29) Shen, T. Z.; Hong, S. H.; Lee, B.; Song, J. K. Bottom-Up and Top-Down Manipulations for Multi-order Photonic Crystallinity in a Graphene-Oxide Colloid. *NPG Asia Mater.* **2016**, *8*, e296.
- (30) Kim, Y. K.; Min, D. H. Preparation of Scrolled Graphene Oxides with Multi-Walled Carbon Nanotube Templates. *Carbon* **2010**, *48*, 4283–4288.
- (31) Wang, X. S.; Yang, D. P.; Huang, G. S.; Huang, P.; Shen, G. X.; Guo, S. W.; Mei, Y. F.; Cui, D. X. Rolling up Graphene Oxide Sheets into Micro/Nanoscrolls by Nanoparticle Aggregation. *J. Mater. Chem.* **2012**, *22*, 17441–17444.
- (32) Zeng, F. Y.; Kuang, Y. F.; Wang, Y.; Huang, Z. Y.; Fu, C. P.; Zhou, H. H. Facile Preparation of High-quality Graphene Scrolls from Graphite Oxide by A Microexplosion Method. *Adv. Mater.* **2011**, *23*, 4929–4932.
- (33) Amadei, C. A.; Stein, I. Y.; Silverberg, G. J.; Wardle, B. L.; Vecitis, C. D. Fabrication and Morphology Tuning of Graphene Oxide Nanoscrolls. *Nanoscale* **2016**, *8*, 6783–6791.
- (34) Gao, Y.; Chen, X. Q.; Xu, H.; Zou, Y. L.; Gu, R. P.; Xu, M. X.; Jen, A. K.; Chen, H. Z. Highly-Efficient Fabrication of Nanoscrolls from Functionalized Graphene Oxide by Langmuir–Blodgett Method. *Carbon* **2010**, *48*, 4475–4482.
- (35) Zhao, J. Z.; Yang, B. J.; Yang, Z.; Zhang, P.; Zheng, Z. M.; Ren, W. C.; Yan, X. B. Facile Preparation of Large-Scale Graphene Nanoscrolls from Graphene Oxide Sheets by Cold Quenching in Liquid Nitrogen. *Carbon* **2014**, *79*, 470–477.
- (36) Tang, B.; Xiong, Z. Y.; Yun, X. W.; Wang, X. G. Rolling up Graphene Oxide Sheets through Solvent-Induced Self-assembly in Dispersions. *Nanoscale* **2018**, *10*, 4113–4122.
- (37) Hone, J.; Carpick, R. W. Slippery When Dry. *Science* **2015**, *348*, 1087–1088.
- (38) Mpourmpakis, G.; Tylianakis, E.; Froudakis, G. E. Carbon Nanoscrolls: A Promising Material for Hydrogen Storage. *Nano Lett.* **2007**, *7*, 1893–1897.
- (39) Li, H.; Wu, J. M. T.; Qi, X. Y.; He, Q. Y.; Liusman, C.; Lu, G.; Zhou, X. Z.; Zhang, H. Graphene Oxide Scrolls on Hydrophobic Substrates Fabricated by Molecular Combing and Their Application in Gas Sensing. *Small* **2013**, *9*, 382–386.
- (40) Joshi, R. K.; Carbone, P.; Wang, F. C.; Kravets, V. G.; Su, Y.; Grigorieva, I. V.; Wu, H. A.; Geim, A. K.; Nair, R. R. Precise and Ultrafast Molecular Sieving Through Graphene Oxide Membranes. *Science* **2014**, *343*, 752–754.
- (41) Abraham, J.; Vasu, K. S.; Williams, C. D.; Gopinadhan, K.; Su, Y.; Cherian, C. T.; Dix, J.; Prestat, E.; Haigh, S. J.; Grigorieva, I. V.; Carbone, P.; Geim, A. K.; Nair, R. R. Tunable Sieving of Ions Using Graphene Oxide Membranes. *Nat. Nanotechnol.* **2017**, *12*, 546–550.
- (42) Mi, B. X. Graphene Oxide Membranes for Ionic and Molecular Sieving. *Science* **2014**, *343*, 740–742.
- (43) Braga, S. F.; Coluci, V. R.; Legoa, S. B.; Giro, R.; Galvão, D. S.; Baughman, R. H. Structure and Dynamics of Carbon Nanoscrolls. *Nano Lett.* **2004**, *4*, 881–884.
- (44) Xia, D.; Xue, Q. Z.; Xie, J.; Chen, H. J.; Lv, C.; Besenbacher, F.; Dong, M. D. Fabrication of Carbon Nanoscrolls from Monolayer Graphene. *Small* **2010**, *6*, 2010–2019.
- (45) Iijima, S. Helical Microtubules of Graphitic Carbon. *Nature* **1991**, *354*, 56–58.
- (46) Xie, X.; Ju, L.; Feng, X. F.; Sun, Y. H.; Zhou, R. F.; Liu, K.; Fan, S. S.; Li, Q. Q.; Jiang, K. L. Controlled Fabrication of Highly-quality Carbon Nanoscrolls from Monolayer Graphene. *Nano Lett.* **2009**, *9*, 2565–2570.
- (47) Prakongpan, S.; Nagai, T. Solubility of Acetaminophen in Cosolvents. *Chem. Pharm. Bull.* **1984**, *32*, 340–343.
- (48) Salimi-Moosavi, H.; Cassidy, R. M. Control of Separation Selectivity and Electroosmotic Flow in Nonaqueous Capillary Electrophoretic Separations of Alkali and Alkaline Earth Metal Ions. *J. Chromatogr. A* **1996**, *749*, 279–286.
- (49) Poulin, P.; Jalili, R.; Neri, W.; Nallet, F.; Divoux, T.; Colin, A.; Aboutalebi, S. H.; Wallace, G.; Zakri, C. Superflexibility of Graphene Oxide. *Proc. Natl. Acad. Sci. U. S. A.* **2016**, *113*, 11088–11093.
- (50) Shi, X. H.; Pugno, N. M.; Gao, H. J. Mechanics of Carbon Nanoscrolls: A Review. *Acta Mech. Solida Sin.* **2010**, *23*, 484–497.
- (51) Yin, Q. F.; Shi, X. H. Mechanics of Rolling of Nanoribbon on Tube and Sphere. *Nanoscale* **2013**, *5*, 5450–5455.
- (52) Shi, X. H.; Pugno, N. M.; Gao, H. J. Constitutive Behavior of Pressurized Carbon Nanoscrolls. *Int. J. Fract.* **2011**, *171*, 163–168.
- (53) Xu, Z.; Zheng, B. N.; Chen, J. W.; Gao, C. Highly Efficient Synthesis of Neat graphene Nanoscrolls from Graphene Oxide by Well-Controlled Lyophilization. *Chem. Mater.* **2014**, *26*, 6811–6818.
- (54) Shih, C. J.; Lin, S. C.; Sharma, R.; Strano, M. S.; Blankschtein, D. Understanding the pH-Dependent Behavior of Graphene Oxide Aqueous Solutions: A Comparative Experimental and Molecular Dynamics Simulation Study. *Langmuir* **2012**, *28*, 235–241.
- (55) Wu, L.; Liu, L.; Gao, B.; Muñoz-Carpena, R.; Zhang, M.; Chen, H.; Zhou, Z. H.; Wang, H. Aggregation Kinetics of Graphene Oxides in Aqueous Solutions: Experiments, Mechanisms, and Modeling. *Langmuir* **2013**, *29*, 15174–15181.
- (56) Zhao, J. P.; Pei, S. F.; Ren, W. C.; Gao, L. B.; Cheng, H. M. Efficient Preparation of Large-Area Graphene Oxide Sheets for Transparent Conductive Films. *ACS Nano* **2010**, *4*, 5245–5252.
- (57) Zhou, X. F.; Liu, Z. P. A Scalable, Solution-Phase Processing Route to Graphene Oxide and Graphene Ultralarge Sheets. *Chem. Commun.* **2010**, *46*, 2611–2013.

- (58) Xiong, Z. Y.; Liao, C. L.; Han, W. H.; Wang, X. G. Mechanically Tough Large-Area Hierarchical Porous Graphene Films for High-Performance Flexible Supercapacitor Applications. *Adv. Mater.* **2015**, *27*, 4469–4475.